Preprints of the 19th World Congress
The International Federation of Automatic Control
Cape Town, South Africa. August 24-29, 2014

Jerk and Current Limited Flatness-based Open Loop Control of Foveation Scanning Electrostatic Micromirrors

Richard Schroedter*, Klaus Janschek, Thilo Sandner***

** Fraunhofer Institute for Photonic Microsystems (FhG-IPMS), AMS, Microscanner R&D, Dresden, Germany, (e-mail: richard.schroedter@ipms.fraunhofer.de).*
*** Institute of Automation, Faculty of Electrical and Computer Engineering, Technische Universität Dresden, Dresden, Germany (e-mail: klaus.janschek@tu-dresden.de)*

Abstract: This paper describes open loop control measures for performance improvements of electrostatic micromirrors in context with foveation scanning for 3D time-of-flight cameras. The generation of high accuracy scanning trajectories with scene dependent variable slope is realized by a flatness-based open loop control scheme. Previous flatness-based control solutions have shown unfavorable residual oscillations excited at slope reverse points and high drive currents at zero-crossing comb deflection due to square-root voltage law for electrostatic mirror control. Jerk limited trajectories are introduced for reduction of residual oscillations and their impact on scanning trajectory properties is expressed by design formulas. A considerable reduction of zero-crossing drive currents can be achieved by using a dual-comb control law at small deflection angles reducing the effective drive voltage slope. The paper addresses the basic micromirror models and describes in detail the jerk and current limitation control measures in context with the flatness-based control concept. Experimental results prove the adequacy of the proposed solutions.

1. INTRODUCTION

The current paper describes the open loop control of the scanning function of a novel 3D time-of-flight (TOF) laser camera with foveation properties for robotic applications [1]. Foveated imaging denotes a higher image resolution at specific regions of interest. In the current design this is realized by adapting the scanning speed of a micromirror assembly within a range of typ. 10 Hz.

The core element of the laser camera is an innovative laser scanning 2D-micromirror assembly, developed at Fraunhofer Institute for Photonic Microsystems (FhG-IPMS), based on a two-stage gimballed electrostatic comb transducer [2], a schematics view is given in Fig. 1. The inner cardanic axis is operating in resonant-mode at 1600 Hz, whereas the outer axis (typ. eigenfrequency 123 Hz) is formed by a vertical comb structure in a so-called Staggered Vertical Comb (SVC) configuration that allows quasistatic operation with large deflection angles, typ. ±10° (cf. Fig. 2a). A micromirror with elliptic aperture of 2.6x3.6 mm² is mounted on the inner axis silicon plate (cf. Fig. 2b). An example for typical scanning trajectories with variable slope is shown in Fig. 3.

The command tracking of a quasistatic micromirror axis is challenged in general by the inherently nonlinear transducer characteristics and the extremely lightly damped mass-spring dynamics.

Closed loop control is employed less for such MEMS-devices (MEMS – micro-electro-mechanical systems), mainly for technological simplicity, i.e. for avoiding additional sensing devices [3]. Open loop control concepts in general rely fundamentally on accurate models of MEMS dynamics.

A common commanding technique using linear model dynamics is input shaping, where the lightly damped eigenmode oscillations are smoothed out by destructive interference of pulse-shaped command inputs, e.g. [4,5]. Another rather straightforward approach is prefiltering of the commanded trajectory profiles by some compensating prefilter with inverse microscanner dynamics, e.g. [6]. For the current application linear solutions show moderate performances with still residual oscillations due to imperfect cancellation of the nonlinear mass-spring microscanner dynamics [6]. Due to the nonlinear microscanner system dynamics it is worth investigating alternative nonlinear command tracking techniques. In this context the flatness-based design paradigm [7] is a very promising candidate; it has been applied to some MEMS applications, e.g. [8] and it has been successfully adopted for the MEMS microscanner investigated here [9]. The results in [9] demonstrate, as to be expected, considerable performance improvements w.r.t. the linear approaches described in [6], however unfavorable residual oscillations excited at slope reverse points and high drive currents at zero-crossing comb deflection due to square-root voltage law for electrostatic mirror control are still existing.

The contributions of this paper comprise performance improvements w.r.t. flatness-based control laws given in [9] by applying (i) limited jerk trajectories for reduction of residual oscillations and (ii) a dual-comb control law at small deflection angles for reduction of drive currents. The design solutions have been successfully verified on a real microscanner assembly.

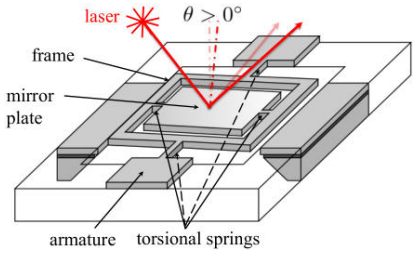

Fig. 1. Principle of laser light deflection with 2D gimballed micro mirror

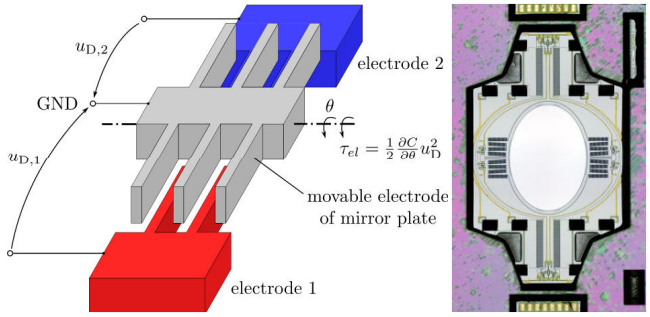

Fig. 2. (a) Schematic configuration of quasistatic microscanner with staggered vertical comb (SVC) drive, (b) Photograph of quasistatic / resonant 2D-Microscanner developed by FhG-IPMS

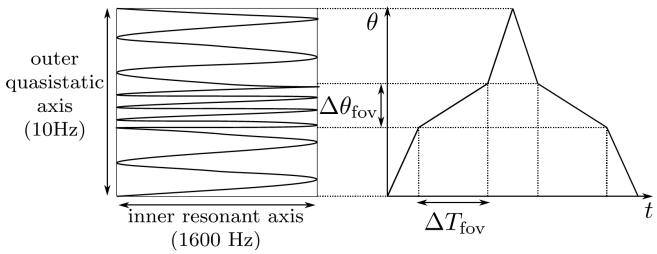

Fig. 3. Mirrors 2D deflection scheme using foveation trajectories for outer quasistatic axis

2. MICROSCANNER DESIGN MODEL

The nonlinear microscanner system dynamics can be denoted by torque equilibrium:

$$\tau_{\text{eff}} := J\ddot{\theta} + b\dot{\theta} + \tau_{\text{spring}}(\theta) = \frac{1}{2}C_1'(\theta)u_{D,1}^2 + \frac{1}{2}C_2'(\theta)u_{D,2}^2 . \quad (1)$$

with the model parameters $J = 4.35 \cdot 10^{-12}\,\text{kgm}^2$ for mirror inertia, $b = 3.3 \cdot 10^{-11}$ Nms/rad for viscous damping and $C_i' := \partial C_i(\theta)/\partial\theta$. The driving voltage $u_{D,1}, u_{D,2}$ is restricted to $\pm 150\,V$. An ANSYS analysis of the microscanner provides the nonlinear progressive spring stiffness, shown in Fig. 5b. Consequently, the nonlinear spring torque is denoted by:

$$\tau_{\text{spring}}(\theta) = \int_0^\theta k(\theta')d\theta' . \quad (2)$$

The static deflection characteristic $\overline{u}_D(\theta)$ can be measured at stationary conditions $(\dot{\theta}, \ddot{\theta} = 0)$, measurement results are shown in Fig. 4 for single sided actuation.

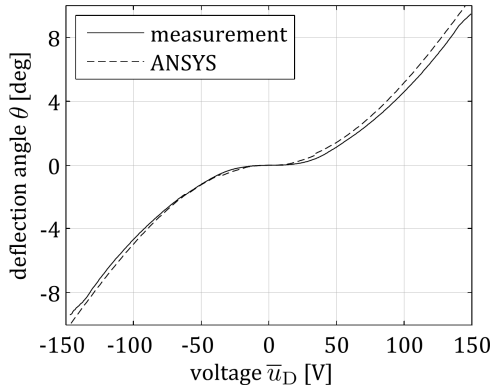

Fig. 4. Static deflection characteristic curve

The quasistatic comb drive capacitance derivatives, shown in Fig. 5a, have been determined by measuring the static deflection characteristic and solving (1) separately, i.e. for comb 1 (equivalent computations for comb 2):

(a) *single comb actuation* for positive deflection angles

$$C_1'(\theta) = \frac{2\tau_{\text{spring}}(\theta)}{\overline{u}_{D,1}^2(\theta)} \quad \text{for} \quad \theta \geq 0 \quad \text{and,} \quad (3)$$

(b) *dual comb actuation* for negative deflection angles, when the comb is emerged (i.e. opposite comb is immersed), using correspondent $C_2'(\theta)$ from *single comb actuation*

$$C_1'(\theta) = \frac{2\tau_{\text{spring}}(\theta)}{\overline{u}_{D,1}^2(\theta)} - C_2'(\theta)\frac{\overline{u}_{D,2}^2(\theta)}{\overline{u}_{D,1}^2(\theta)} \quad \text{for} \quad \theta < 0 . \quad (4)$$

The reassembled capacitance derivative curves are shown in Fig. 5a. Therein the singularity at zero deflection angle is replaced by a linear interpolation. The region of very small values of capacitance derivative has been exponentially extrapolated. This is the deflection region, where the comb is emerged and the deflection could not be measured, because of too small torques.

The important property of this comb arrangement is that even at small angles with emerged comb figures there is still torque authority with that emerged comb finger. This allows a *dual comb actuation* with opposing (bipolar) torques around zero deflection region (cf. section 4).

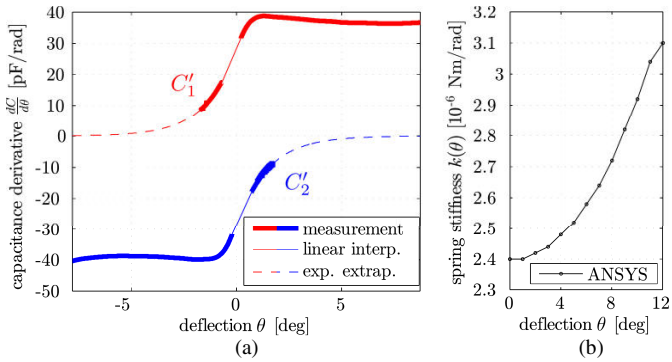

Fig. 5. Comb characteristics as a function of the mirror deflection angle: (a) capacitance derivatives, (b) nonlinear torsional spring stiffness

3. JERK-LIMITED FLATNESS-BASED TRAJECTORY DESIGN

The flatness-based open loop control, presented in [9], allows a systematic command trajectory design for quasistatic microscanner with extremely lightly damped mechanical mass-spring system. The control scheme is sketched in Fig. 6. The deflection angle θ was chosen as *flat output* z, hence the input $u_D = u_r$ complies with the nonlinear driving function law as follows:

$$\theta(z) = z$$
$$u_r(z,\dot{z},\ddot{z}) = \sqrt{\frac{2}{C'(z)}\left(J\ddot{z} + b\dot{z} + \tau_{spring}(z)\right)}. \quad (5)$$

According to the highest time derivatives of the input $(n=2)$ and output $(q=0)$ in (5), the *relative degree* is defined as the difference $r = n - q = 2$. Any desired command trajectory must be r-times continuously differentiable, and therefore, in this case, the command deflection angle θ_r require continuity until the second derivative.

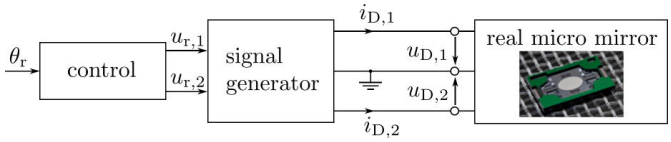

Fig. 6. Control scheme for quasistatic axis of microscanner

The application of fifth order polynomials for rounding off discontinuities of triangle shaped command trajectories gives no inherent restriction to reduce residual mirror oscillation, caused by small uncertainties of the microscanner model.

It has been shown that the level of jerk, i.e. third time derivative of displacement, has a strong influence on the joint position errors of robot manipulators, i.e. reduced jerk means smaller errors [10]. This leads to minimum jerk trajectory generation schemes, motivated also from biological systems (muscle movements, c.f. [11]) and has been applied successfully to mechatronic applications, e.g. [12].

For the current micro mirror system we will not follow the minimum jerk approach, but rather specify a *hard jerk limit* – *jerk maximum magnitude* j_{max} – as a design parameter. This jerk-limited trajectory design approach allows linking the maximum trajectory jerk with the tracking errors of the mirror deflection. The following third-order polynomial describes the deflection trajectory approach with the allowed maximum jerk magnitude j_{max} and the constants θ_0 (initial deflection), $\dot{\theta}_0$ (initial velocity):

$$\theta(t) = \theta_0 + \dot{\theta}_0 t + \frac{j_{max}}{6} t^3 . \quad (6)$$

The triangle shaped movement in Fig. 7 is a typical command trajectory for quasistatic microscanners with the region of interest (ROI) incorporated in the linear scanning area $\pm\theta_{lin}$. The maximum mirror deflection (maximum angle of the ideal triangle) is denoted by $\pm\theta_{max}$.

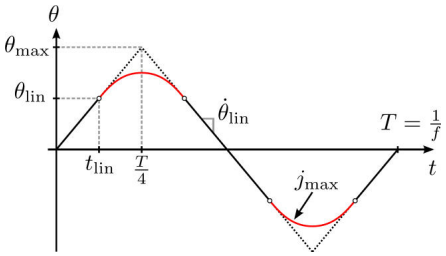

Fig. 7. Jerk limited triangle trajectory

The maximum jerk magnitude j_{max} can be parametrized using the general relation between the maximum deflection θ_{max}, the ratio of linear scanning area $k_{lin} := \theta_{lin} / \theta_{max}$ and the trajectory frequency f:

$$|j_{max}| = \frac{128}{(1-k_{lin})^2}\theta_{max} f^3 . \quad (7)$$

Figure 8 shows the shaped trajectory for a 10 Hz triangle trajectory in the range of $\theta_{max} = 7°$ with variation of the linear scanning area; the equivalent jerk limitations and tracking errors (experimental results) are given in Table 1. The results show a proportional relationship between maximum jerk magnitude and peak-to-peak tracking error. Thus the expression (7) together with the experimental results from Table 1 simplify the triangle trajectory design and allow a transparent parametric prediction of the mirror residual oscillations according to the given jerk limitation or the linear scanning area.

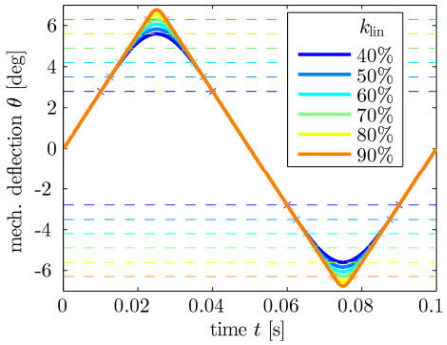

Fig. 8. Variation of ROI linear area k_{lin} and jerk-limitation for a typical triangle command trajectory with 10 Hz and $\theta_{max} = 7°$

4. LIMITED DRIVE CURRENT TRAJECTORY DESIGN

The flatness-based command tracking design, as presented in the previous paper [9], implements only a single sided comb actuation. Equation (8) expresses the flatness-based command voltage for both combs, where only the positive deflection side of the capacitance derivative C_1' and negative deflection side of C_2' are utilized for torque generation:

$$u_D = \begin{cases} \sqrt{\frac{2}{C_1'}\tau_{eff}}, & \theta \geq 0 \\ -\sqrt{\frac{2}{|C_2'|}\tau_{eff}}, & \theta < 0 \end{cases} . \quad (8)$$

At zero crossing point the drive torque becomes almost zero $\tau_{\text{eff}}(\theta = 0) \approx 0$ due to the static deflection characteristics $\overline{u}_D(\theta = 0) = 0$, (Fig. 9). Therefore, the root function in (8) leads to very steep voltage slope, which causes large current peaks $i_{\text{D}} = C_0 \dot{u}_{\text{D}}$ due to stray capacitance C_0, as shown in Fig. 9.

As visible from the system model (1) each comb can generate nominally only a unidirectional torque according to the square-law for voltage control. However the special characteristics of the comb capacitance derivative function implies a simultaneous dual torque authority with opposing torques by both combs around zero mirror deflection (cf. Fig. 5a : negative deflections for comb 1, positive deflections for comb 2). Therefore opposing torques can be applied by both combs offering the advantage of two-sided actuation and incorporating an additional degree of freedom for control design.

Current limitation for capacitive loads can be achieved in general by limiting the command voltage slope. For a given maximum slope $\dot{u}_{\text{max}}$ the original command voltage trajectory can be extrapolated linearly at a maximum voltage slope (cf. Fig. 10). Starting at the initial voltage $u^0_{\text{D,lin}}$, that first exceeds the slope limit $\dot{u}_{\text{max}}$, the linear command voltage law can be stated as:

$$\begin{aligned} u_{\text{D,lin}} &= -\dot{u}_{\text{max}} t + u^0_{\text{D,lin}} \\ t \geq t^*, \quad t^* &: \frac{d}{dt} u_{\text{D}}(t^*) > \dot{u}_{\text{max}} \end{aligned} . \tag{9}$$

For a linear command voltage $u_{\text{D,lin,1}}$ at comb 1 the opposing comb drive voltage $u_{\text{D,2}}$ must be applied as

$$u_{\text{D,2}} = \sqrt{\frac{2}{C_2'} \tau_{\text{eff}} - \frac{C_1'}{C_2'} u^2_{\text{D,lin,1}}} . \tag{10}$$

to retain the torque balance of the mechanical system (1) and to follow the demanded deflection trajectory (equivalent computations for comb 2).

The resulting command voltage trajectory, shown in Fig. 10, can comprehend larger voltage derivatives for the opposite comb drive caused by different capacitance characteristics for both combs. Nevertheless the final command voltage trajectory is bounded in contrast to the original single-sided comb actuation with infinity (very large) slope at the zero crossing point.

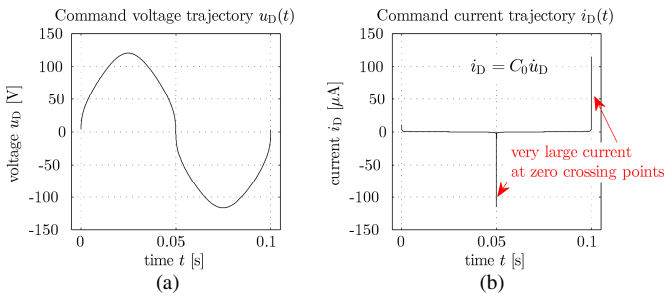

Fig. 9. Command trajectories: (a) voltage trajectory $u_{\text{D}}(t)$, (b) current trajectory $i_{\text{D}}(t)$ showing large displacement current through capacitance C_0 at zero crossing points

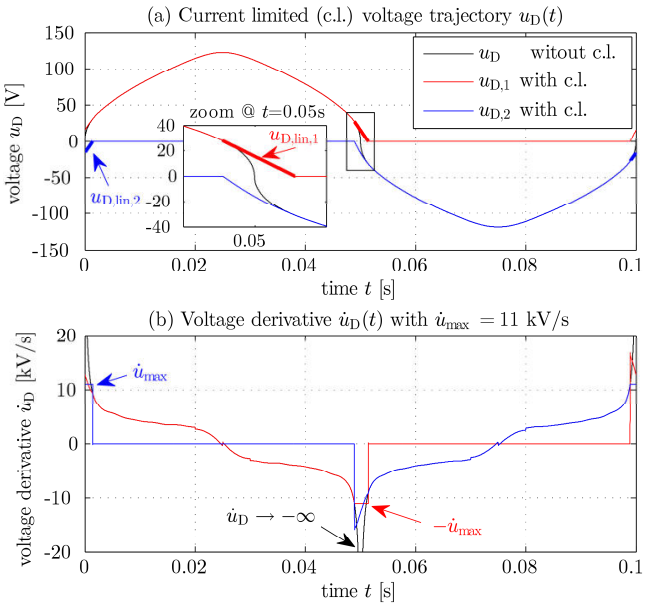

Fig. 10. Current and jerk limited trajectory design with limitation $\dot{u}_{\text{max}} = 11$ kV/s : (a) voltage trajectory with/without current limitation (c.l.), the linear extrapolated parts of trajectory are indicated with bold line; (b) voltage derivatives of upper voltage trajectories

The benefits of limiting the drive current can be accounted for (i) reducing the power amplifier (voltage generator) requirements and (ii) diminishing electrical cross-talk, which indicates a problem for on-chip piezoresistive position sensors that are planned to be used for feedback control.

5. EXPERIMENTAL RESULTS

The experimental validation has been conducted with a microscanner [1,2] in a test setup shown in Fig. 11. Command voltage trajectories were created with a two channel programmable voltage generator and amplifier. An external optical reference measurement of the mirror deflection angle has been performed with a position sensitive detector (PSD). The measurement equation (11) for the mirror deflection angle is given as:

$$\hat{\theta} = \frac{1}{2} \arcsin\left(\frac{k_{\text{PSD}}}{d} \frac{I_a - I_b}{I_a + I_b} \right), \tag{11}$$

with the displacement currents I_a, I_b, the calibration factor k_{PSD} and the distance d between PSD and micro mirror. The drive current i_{D} was measured in the ground wire.

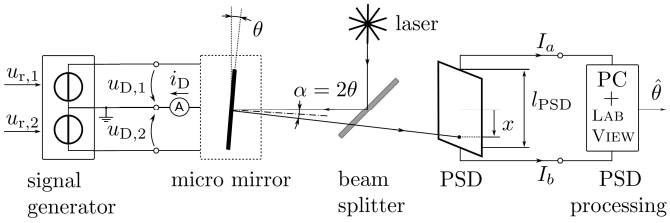

Fig. 11. Experimental setup for measurement of mirror deflection angle

5.1. PERFORMANCE OF JERK LIMITATION

The performance of jerk-limited trajectory design is verified with triangle trajectories and a variation of the linear scanning area according to Fig. 8. The measurement results, demonstrated in Table 1 prove the feasibility of the proposed design approach for decreasing the mirror tracking error. By reducing the maximum jerk magnitude the mirror deflection tracking error can be reduced considerably. At the same time the repeatability, defined as the deviation from the mean deflection of 100 periods, persists approximately constant at a very small error level.

Comparing the jerk-limited design with the polynomial design shown in [9], the jerk-limited trajectory design improves the performance by reducing the maximum jerk by 37%, cf. third to last with last row in Table 1. This leads to a smaller error and a better repeatability, mentioning, that different mirror devices were used for both measurements.

Some residual oscillations at the micro mirror outer eigenfrequency of 123 Hz due to unavoidable inaccuracies of the design model can be recognized in the measured mirror deflections for $k_{\text{lin}} = 40\%$ (cf. Fig. 12).

Best performances with jerk limited trajectories can be achieved by minimizing the jerk magnitude and as an unavoidable side effect the linear scan area. This is in conflict with a maximal admissible linear scanning area for the microscanner that is restricted by the geometric micro mirror design. Thus a compromise must be found. Relation (7) can be used for a transparent parameterization of the command deflection trajectory with respect to the admissible error tolerances of the mirror motion.

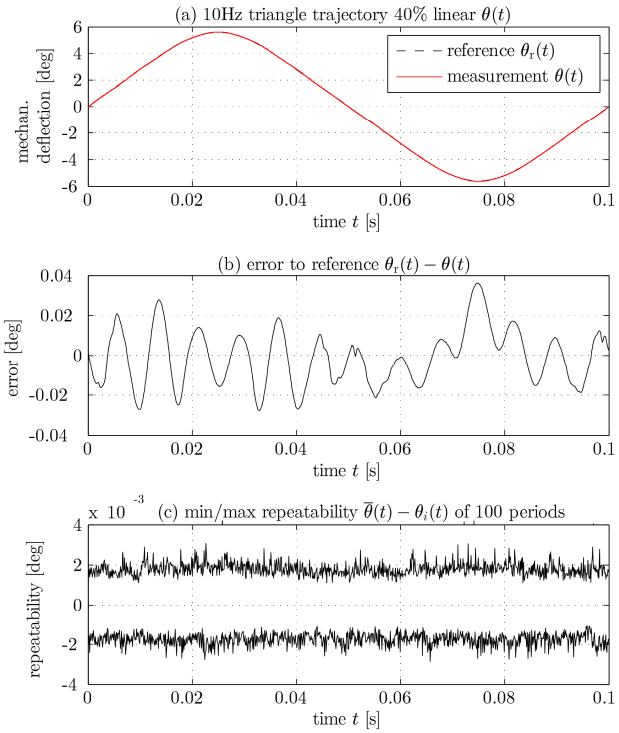

Fig. 12. Measurement result of jerk-limited 10 Hz triangle trajectory with 40% linear area and $\theta_{\max} = 7°$: (a) reference and measurement, (b) error to reference, (c) minimum and maximum repeatability of 100 periods

Table 1. Measurement results for 10 Hz jerk-limited triangle trajectory at $\theta_{\max} = 7°$ with 100 periods (cf. Fig. 8): peak-to-peak error to reference and peak-to-peak repeatability (deviation to mean at each time)

linear area k_{lin} [%]	jerk limitation $j_{\max}$ [deg/s^3]	peak-to-peak error [deg]	peak-to-peak repeatability [deg]
40	$2.5 \cdot 10^6$	0.0695	0.0065
50	$3.6 \cdot 10^6$	0.1063	0.0070
60	$5.6 \cdot 10^6$	0.1324	0.0063
70	$10.0 \cdot 10^6$	0.1538	0.0067
80	$22.4 \cdot 10^6$	0.1971	0.0069
90	$89.6 \cdot 10^6$	0.3015	0.0072
80	$30.7 \cdot 10^{6\,**}$	0.2330*	0.0275*

* [9, Table 1] (without standardization to max. deflection)
** denotes the maximum jerk of trajectory design from [9]

5.2. PERFORMANCE OF CURRENT LIMITATION

The drive current limiting trajectory design is verified by current measurement in the ground wire. The exemplary current measurement for a jerk-limited, 80% linear, 10 Hz triangle trajectory with the design parameter $\dot{u}_{\max} = 101\ \text{kV/s}$ (maximum voltage slope) is shown in Fig. 13. It indicates that the drive current is mainly influenced by the constant stray capacitance C_0. Thus, the drive current can be expressed by:

$$i_{\text{D}} \approx C_0 \dot{u}_{\text{D}}. \tag{12}$$

Figure 13 illustrates the current peaks at mirror deflection zero crossing time at $t = 0.05\text{s}$. A reloading of the comb capacitances is required resulting in an unfavourable electrical coupling from the supply conductor to the integrated piezoresistive sensors.

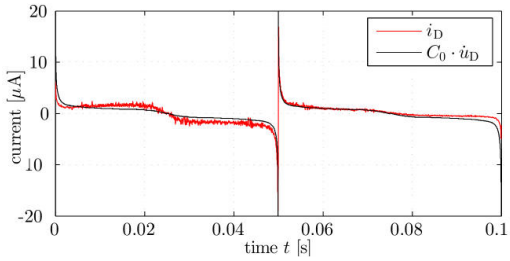

Fig. 13. Current measurement for jerk-limited 80% linear 10 Hz triangle trajectory with limited $\dot{u}_{\max} = 101\ \text{kV/s}$, $\theta_{\max} = 7°$ and calculated command voltage derivative (12), with $C_0 = 243\ \text{pF}$

The proposed current limiting trajectory design achieves the predicted current depression as an almost linear function of the design parameter $\dot{u}_{\max}$, see measured results in Fig. 14. Here, the measurement equation for the maximum current is determined by the upper and lower limit of the mean of 100 periods as follows:

$$\bar{i}_{\text{D,max}} = \frac{1}{2}\left[\max(\bar{i}_{\text{D}}) - \min(\bar{i}_{\text{D}})\right],\ \bar{i}_{\text{D}} = \frac{1}{100}\sum_{i=1}^{100} i_{\text{D},i}\,. \tag{13}$$

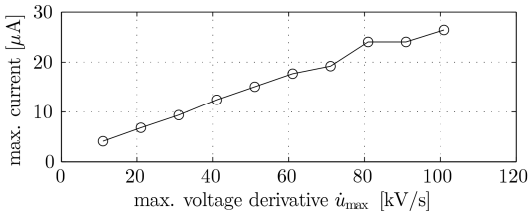

Fig. 14. Measurement result of maximum current $\overline{i}_{D,max}$ (13) at zero crossing point for variation of maximum voltage derivative $\dot{u}_{max}$

Above all the mechanical scanning performance should not be affected or even worsened. An experimental analysis demonstrates (results are shown in Fig. 15) that the mirror tracking error for a jerk-limited 80% linear 10 Hz triangle trajectory with current limitation persists in the range of $\pm 0.1°$ at a repeatability of $\pm 0.01°$ (cf. Table 1, third to last row).

Finally the dual-comb actuation scheme has been implemented successfully to limit the drive current, but shows also prospective optimization potentials for future feedback control schemes.

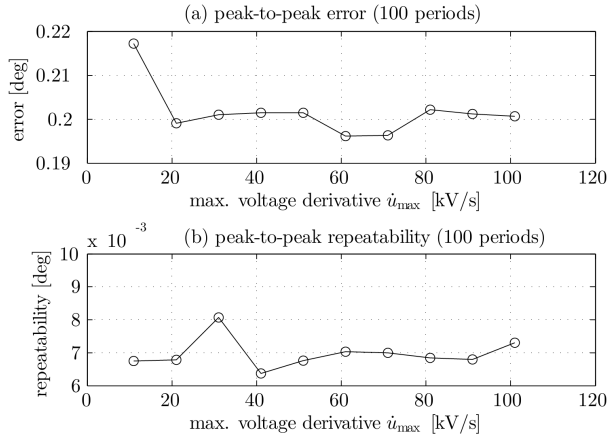

Fig. 15. Measurement errors for 100 periods of a jerk-limited 80% linear 10 Hz triangle trajectory with variation of max. voltage derivative $\dot{u}_{max}$: (a) peak-to-peak error to reference, (b) peak-to-peak repeatability

6. CONCLUSIONS

This paper presented performance improvements for open loop electrostatic micromirror control using a flatness-based trajectory design with limited jerk and limited drive currents. The experimental verification proves the adequacy of the proposed solutions. Although the model-based open loop control shows rather satisfying performances there are still some open issues for improving the system performances (reduction of tracking errors) and enhancing the robustness. Improving the micromirror model accuracy would be a rather straightforward approach, but would be beneficial eventually only for optimized design of a specific micromirror assembly requiring comprehensive experiments for model parameter extraction (cf. sect. 2). In order to minimize individual experiments we are more interested in robust system concepts allowing certain model and parameter uncertainties.

To gain robustness for the weakly damped mass-spring eigenmode an artificial damping, either passively through resistive impedance feedback [6,9] or actively using piezoresistive deflection sensors (already integrated on-chip, but not used so far) will be investigated further. For both variants the solutions presented in this paper for lowering of drive currents are of crucial importance.

REFERENCES

[1] Thielemann, J., Sandner, T., Schwarzer, S., Cupcic, U., Schumann-Olsen, H., Kirkhus, T., 2010. „TACO: Three-dimensional Camera with Object Detection and Foveation", EC FP7 grant no 248623, http://www.taco-project.eu/

[2] Jung, D., Sandner, T., Kallweit, D., Schenk, H., 2012."Vertical comb drive microscanners for beam steering, linear scanning, and laser projection applications". In: Proc. SPIE 8252, MOEMS and Miniaturized Systems XI, 82520U (February 9, 2012); doi:10.1117/12.906690.

[3] Ferreira, A., Aphale, S.S., 2011. "A Survey of Modeling and Control Techniques for Micro- and Nanoelectromechanical Systems", IEEE Transactions on Systems, Man, and Cybernetics—Part C: Applications and Reviews, Vol. 41, No. 3, pp. 350-364.

[4] Singer, N.C.; Seering, W.P., 1990. "Preshaping Command Inputs to Reduce System Vibration". Trans. ASME, J. Dyn. Syst. Meas. Control, vol. 112, no. 1, 1990, pp. 76–82.

[5] Ou, K.-S.; Chen, K.-S.; Yang, T.-S.; Lee, S.-Y., 2011. "Fast Positioning and Impact Minimizing of MEMS Devices by Suppression of Motion-Induced Vibration by Command-Shaping Method". Journal of Microelectro¬mechanical Systems, Vol. 20 (2011), No.1, pp. 128 –139.

[6] Janschek, K.; Sandner, T.; Schroedter, R.; Roth, M., 2013. "Adaptive Prefilter Design for Control of Quasistatic Microscanners". In: Proceedings of 6th IFAC Symposium on Mechatronic Systems – Mechatronics '13, April 10-12, 2013, Hangzhou, China, doi:10.3182/20130410-3-CN-2034.00112, pp. 197-206.

[7] Fliess, M., Lévine, J. and Rouchon, P. , 1995. "Flatness and defect of nonlinear systems: Introductory theory and examples", International Journal of Control, 1995, vol. 61, pp. 1327-1361.

[8] Zhu, G.; Levine, J.; Praly, L.; Peter, Y.-A., 2006. "Flatness-Based Control of Electrostatically Actuated MEMS With Application to Adaptive Optics: A Simulation Study". J.of Microelectromechanical Systems, Vol. 15 (2006), Issue 5, pp. 1165-1174.

[9] Janschek, K.; Schroedter, R., Sandner, T.; 2013. "Flatness-Based Open Loop Command Tracking for Quasistatic Microscanners". Paper WeAT3.1, 2013 ASME Dynamic Systems & Control Conference (DSCC), October 21-23, 2013, Stanford University, CA, USA.

[10] Kyriakopoulos, K. J.; Saridis, G. N.; 1988. "Minimum jerk path generation," in Proc. IEEE Int. Conf. Robotics and Automation, vol. 1, Philadelphia, PA, 1988, pp. 364–369.

[11] Hogan, N.; 1984. "An organizing principle for a class of voluntary movements". The Journal of Neuroscience, November 1984, Vol. 4, No. 11, pp. 2745-2754

[12] Numasato, H.; Tomizuka, M.; 2003. "Settling Control and Performance of a Dual-Actuator System for Hard Disk Drives". IEEE/ASME Transactions on Mechatronics, Vol. 8, No. 4, December 2003, pp. 431-438.